Journal of Microelectronics and Electronic Packaging (2020) **17**, 28-33

ISSN: 1551-4897

A Technique for Detecting Moisture Absorption in Printed Circuit Boards

Jeffery D. Craven, II, Ariel R. Oldag, and Robert N. Dean*

***Abstract*—Most circuit boards operate in environments that have the potential to be exposed to moisture, either in vapor or liquid form. Because low-cost circuit boards can readily absorb moisture, this can lead to performance issues, reliability issues, and even catastrophic failure. However, it is difficult to detect if moisture absorption has occurred before the circuit board suffers a complete failure. To alleviate this issue, a fringing field capacitor was implemented in printed circuit board (PCB) technology and used to detect the absorption of moisture in the circuit board through the accompanying increase in capacitance. Prototype sensors were fabricated and immersed for 42 d, demonstrating an increase in capacitance of between 14% and 29%. This sensor technology can easily be added to circuit board designs because they use the standard materials and fabrication processes used in commercial PCB construction.**

***Keywords*—Moisture absorption, printed circuit board, packaging**

Introduction

Traditional laminated printed circuit board (PCB) technologies, such as FR-4, can absorb moisture from the operating environment [1]. Some operating environments are particularly harsh and can expose the PCB to large amounts of moisture. These harsh applications include vehicles [2], ships [3], electrical power transmission and distribution systems [4], and alternative energy systems [5]. Specific examples of applications where circuit boards may be exposed to excessive amounts of moisture include vehicle engine controllers, handheld military electronics, and electronics associated with outdoor utility systems. Several deleterious effects can occur if moisture is absorbed by a PCB, including PCB material degradation, delamination, electrical shorting, ionic corrosion, conductive filament formation, and even biofouling [6]. Although various board coatings have been developed to insulate PCBs from exposure to environmental moisture, it is difficult to evaluate the effectiveness of these coatings during circuit operation in the field. Furthermore, it is often difficult to determine if moisture has been absorbed into a PCB before catastrophic failure occurs. Presented here is a moisture detection sensor that comprises the PCB materials themselves. This sensor detects absorbed moisture by using the high dielectric constant of water to affect a fringing field capacitor implemented under the solder mask layer on the PCB. The remainder of this article presents this work.

The manuscript was received on January 1, 2019; revision received on February 12, 2020; accepted on February 13, 2020
Auburn University, 200 Broun Hall, Auburn, Alabama 36830
*Corresponding author; email: deanron@auburn.edu

Background

A. Moisture and Moisture Absorption

The vast majority of terrestrial operating environments afford exposure to moisture. Most of these environments, however, are rather benign. In harsh environments where moisture exposure is an issue, the properties of water can have several effects on electronic systems. Although pure water has a high resistivity [7], water is a polar compound and has an affinity for dissolving ionic compounds. The dissolved ions act as mobile charge carriers, greatly reducing the resistivity of the resulting aqueous solution, even to the point of being able to short conductors. Water possesses a relatively high dielectric constant, 81 at room temperature [8], which increases the capacitance between conductors. The surface tension of water is high compared with many other liquids [9]. As a result, the capillary action of water can cause it to be drawn into cracks and small crevices. Sometimes, it results in hygroswelling [10]. If the water freezes, it will expand as ice forms, enlarging the cracks. Water also facilitates chemical changes on surfaces in contact with it, such as corrosion. In addition, water can facilitate biological organisms that can foul and otherwise affect surfaces and assemblies [11].

B. Moisture Absorption in FR-4 Printed Circuit Board Laminate

Pecht et al. [6] modeled the absorption of moisture in various PCB laminate materials, including FR-4, and developed an approximate equation for the diffusivity of moisture into the circuit board material. From empirical data, they were able to model the equilibrium moisture content of FR-4 by

$$M_{\text{inf}} = .006(\text{RH}) - 3.59\left(10^{-3}\right)(T) + .071, \qquad (1)$$

where M_{inf} is the equilibrium moisture content, RH is the relative humidity (40% $\leq$ RH $\leq$ 85%), and T is temperature (40°C $\leq$ T $\leq$ 85°C). The applicable ranges for RH and T covered only the ranges of relative humidity and temperature investigated in that study. The three coefficients in (1) were averaged from the measurements from testing FR-4 from two different suppliers. Observe that the amount of absorbed moisture in FR-4 increases in a wetter environment, and slightly

doi:10.4071/imaps.1014123

decreases as environmental temperature increases. Assuming that the diffusion is Fickian such that the circuit board of thickness, L, is exposed to the same moist environment on both sides, the initial diffusivity, D, can be approximated using the following equation:

$$\frac{M_t}{M_{\text{inf}}} = \frac{4}{L}\left(\frac{Dt}{\pi}\right)^{.5}, \tag{2}$$

where t is time and M_t is the percent moisture content at time t. If M_t is plotted versus the square root of time, the initial slope of that trace is k. Using k, (2) can be rewritten as follows:

$$D = \pi\left(\frac{kL}{4M_{\text{inf}}}\right)^2. \tag{3}$$

Using (3) with their test data from evaluating FR-4 laminates at 40°C and 85°C and at 50% RH and 85% RH, Pecht et al. [6] reported observed diffusivities between .74 and 3.22 cm^2/s. In addition, other factors would likely affect how fast moisture diffuses into an FR-4 PCB, including proximity to the edge of the board, features of the circuit board design such as ground planes and solder mask coatings, and processing history including reflow cycles.

C. Printed Circuit Board Sensors

Commercial PCB technology is being used to realize a variety of low-cost sensors. Consider the illustration of the two-layer PCB sensor shown in Fig. 1. The nonconductive FR-4 substrate forms a rigid backbone for the sensing electrodes on either side of the PCB. The patterned Cu cladding is used for the sensing electrodes and any required signal traces attached to interface electronics. The polymeric solder mask is used as a thin insulating layer. Four electrodes covered with solder mask are shown on the top side, where the solder mask electrically insulates them from the sensing environment outside of the circuit board. These electrodes can be used to measure the electrical permittivity or the electrical permeability of the surrounding media. Two exposed electrodes are shown on the bottom side, which can be used to measure the resistance and, therefore, the electrical conductivity or resistivity of the surrounding media. By measuring these electrical properties while in the surrounding environment, useful information about the environment can be determined. Examples include the measurement of salinity [12], soil moisture content [13], nitrate concentration [14], pH [15], water supply contamination [16], and the mass of a drop of water [17].

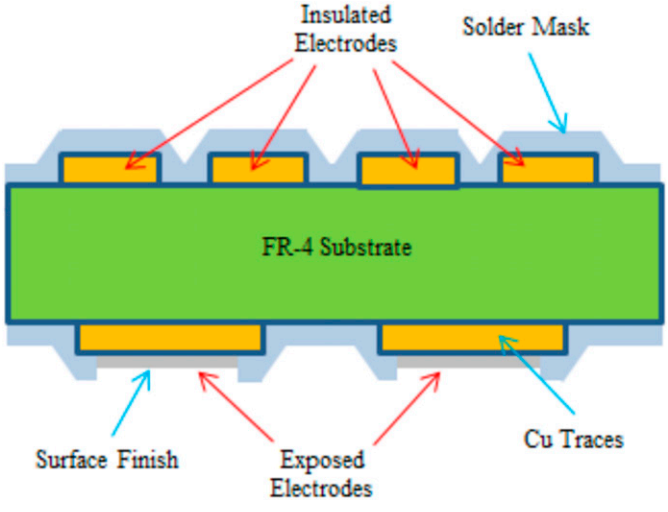

Fig. 1. An illustration of the side view of a PCB sensor.

Sensor Theory

Consider the interdigitated electrode structure illustrated in Fig. 2 consisting of n electrode pairs. "A" and "B" identify the electrode connection points. Let L be the overlapping length between any two adjacent electrode fingers, t be the electrode thickness (perpendicular to the drawing), and d be the separation distance between any two adjacent electrode fingers.

Assuming that L is much larger than either t or d, and if t is much greater than d, then the capacitance between the two electrodes can reasonably be approximated by the following equation:

$$C = \frac{\varepsilon_0 \varepsilon_r L t (n-1)}{d}, \tag{4}$$

where ε_0 is the permittivity of free space, ε_r is the relative permittivity of the homogeneous dielectric material between the electrodes, n is the total number of electrode fingers, and L, t, and d are the structural dimensions illustrated in Fig. 2. For this case, only a negligible amount of the capacitance is due to the fringing fields outside of the volume of the electrode structure. However, now consider the case where t is not significantly greater than d. In this case, a sizable portion of the capacitance between the electrodes is due to the fringing fields outside of the volume of the electrode structure. This results in an increase in the capacitance predicted by (4). To account for this increased capacitance, a fringing factor correction coefficient, γ, is added to (4), resulting in

$$C = \frac{\varepsilon_0 \varepsilon_r L t \gamma (n-1)}{d}, \tag{5}$$

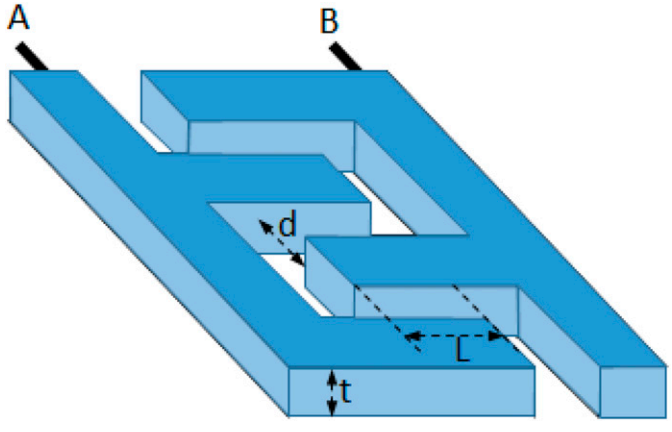

Fig. 2. Cross-sectional illustration of a PCB implemented interdigitated electrode structure.

where γ is greater than or equal to 1. If the default material through which the fringing fields pass through has a relative permittivity of approximately 1, and a material with a much greater relative permittivity enters this volume, the measured capacitance increases accordingly. Because water has a relative permittivity of approximately 81 at room temperature, if water enters this volume, a large increase in capacitance can be achieved [8]. Depending on the geometry of the interdigitated electrode structure, γ can be large. For example, a similar interdigitated electrode structure used as a humidity sensor had a γ of approximately 230 [18]. Because of the difficulty in calculating γ from electromagnetic modeling, it is often easier to determine its value experimentally.

A cross-sectional drawing of an interdigitated electrode configuration depicted in Fig. 2 implemented in PCB technology is presented in Fig. 3. The interdigitated electrodes, "A" and "B," are realized in the patterned Cu cladding on the top side of the PCB. A layer of solder mask completely covers the electrodes and the volume between them. The electric flux lines between the electrodes are shown in Fig. 3 as black dashed lines, illustrating how some of them extend out of the volume of the electrode structure, into the PCB below and into the external region above the PCB. The electric flux lines above the PCB have been used for external sensing applications [8]. In this application, however, the desired sensing environment is the region inside the PCB itself, as illustrated by the electric flux lines extending into the PCB below the electrodes. Moisture absorbed by the PCB in the vicinity of the electric flux lines will result in a measurable increase in the capacitance between the electrodes proportional to the amount of moisture absorbed. The other side of the PCB is available for other circuitry, such as additional interdigitated electrodes, a Cu ground plane, or for the attachment of electronic components. Implementing the moisture absorption sensor in the PCB materials is very convenient for integrating the sensor with its interface circuitry. More complicated PCB sensor configurations could be realized in multilayer PCBs using the inner Cu cladding layers.

At a fixed temperature, this type of sensor produces a linear change in capacitance in proportion to a change in the amount of liquid water present within the sensing volume [13]. PCB-interdigitated electrode capacitive sensors are sensitive to temperature. A similar PCB sensor with a temperature sensitivity in air of .1144% increase in capacitance per degree Celsius relative to 20°C was reported [19]. Also, the relative permittivity of water decreases by approximately .427% for every degree Celsius increase in temperature above 0°C [20]. Therefore, PCB-interdigitated electrode capacitive sensor readings must be referenced to a specific temperature to determine the exact amount of absorbed moisture.

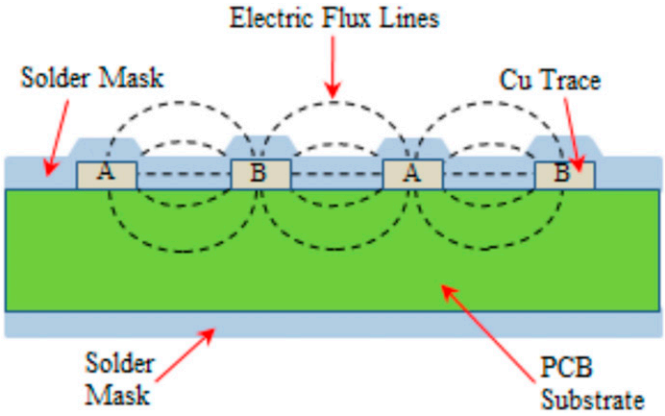

Fig. 3. Illustration of an interdigitated electrode structure.

Senor Design and Fabrication

Prototype sensors were designed to be 2.54 cm in length and width with a thickness of approximately 2.5 mm. There were 72 electrode fingers in each sensor on a circuit board resulting in 36 capacitive fringing pairs, with 152.4 μm (6 mils) spacing between each of the adjacent electrode fingers of the sensor. This resulted in a sensing area on the PCB of approximately 22 mm by 11.4 mm, or 250 mm^2. This area is evident in Fig. 4 by the white silkscreen outline. Below the sensing area were two gold-plated tabs that allowed for electrical connection to the sensor. The backside of the sensor circuit board was just exposed FR-4 material to facilitate moisture absorption for sensor evaluation purposes. The sensor circuit board layout is presented in Fig. 5. Here, blue represents the top patterned copper layer, green represents the top layer silkscreen surrounding the sensing area, and red represents the outline of the board. The solder mask, not shown in the figure, was only applied to the top side and everywhere on that side except over the gold-plated electrical

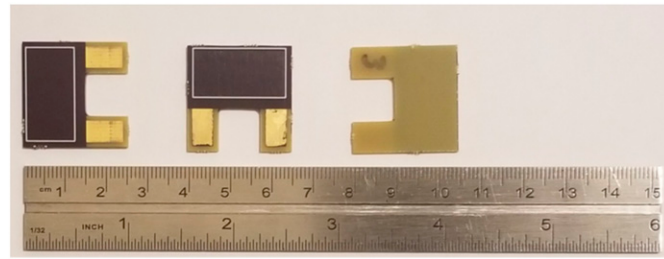

Fig. 4. Photograph of three identical sensor circuit boards.

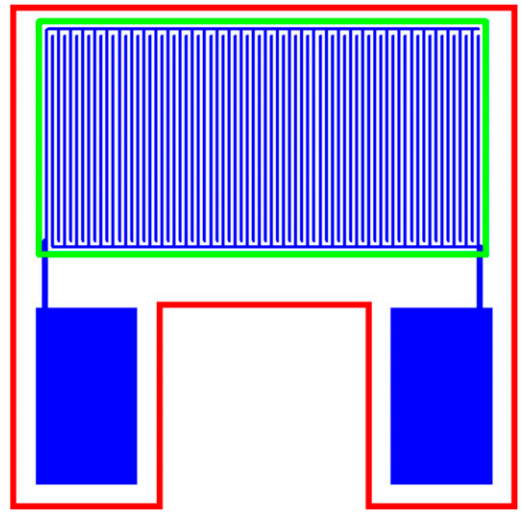

Fig. 5. Layout of the sensor circuit board.

contact pads. The fabrication of the sensors was performed by Osh Park using their standard commercial two-layer FR-4 circuit board fabrication service. Although this prototype only had the sensing structure implemented on it, a PCB that had this sensor with other circuitry would be the intended application. In such an implementation, other features on the circuit board and the sensor's location on the circuit board could affect the sensor's operation and, therefore, must be taken into consideration.

Sensor Testing and Data Analysis

A. Moisture Ingress Testing

The testing of the devices consisted of immersing seven sensors in a glass beaker filled with local tap water for 42 d at room temperature while keeping one PCB outside of the water so as to have a reference to base all measurements on. The complete immersion in water allowed for the quickest water absorption for the boards and to represent an environment where moisture would be at the absolute highest possible value. On a daily basis, each devices' capacitance and conductance were measured in a parallel circuit mode at 100 kHz, 500 kHz, and 1 MHz. The sensors were electrically evaluated using the Agilent 4192A LF Impedance Analyzer, as shown in Fig. 6. Once the sensor capacitance and conductance were measured, the sensors were immediately returned to the water for full immersion until the next day for measurements. For each of the measurements, it can be considered that the temperature for each device was that of room temperature, or approximately 22°C. It should be noted that the devices were not dehydrated before testing, but rather they were dehydrated posttesting instead. This was performed to replicate real world initial conditions of PCBs. Although laboratory instrumentation was used in this investigation to measure sensor capacitance, simple instrumentation techniques, such as integrating the sensor into a Complementary Metal Oxide Semiconductor (CMOS) relaxation oscillator [1, 21], can readily be used.

B. Post Test Dehydration

To remove the moisture located within each of the PCBs after immersion testing concluded, each sensor, including the reference, was placed inside a box oven for approximately 2 h at a temperature of 60°C. This unusually low dehydration temperature ensured that moisture located within the boards was removed without damaging the boards from boiling off the relatively large amounts of absorbed moisture. Once the PCBs had been permitted to cool for approximately 1 h, they were once again tested with the Agilent 4192A at room temperature to measure their capacitance and conductance values.

C. Results

In each case for the measurement of the capacitance and conductance, an increase in the measured values was noticed almost immediately after 1 d of immersion. In general, the rate of increase for these values persisted for the first 5 d before slowing down to a substantially lower rate of absorption in the following days. The collected data for the 42-d testing period can be found in Figs. 7-12. The data for each of the three frequencies evaluated, 100 kHz, 500 kHz, 1 MHz, as well as conductance and capacitance, are graphed separately for the devices and are labeled appropriately. For each graph, the data for each device are shown and a dashed black line representing the device used as a control, in addition to three separate, black dotted lines. The lowest of these dotted lines indicates the lower limit of the standard deviation of the boards. The middle line indicates the grand average for all of the boards. The highest line indicates the upper limit of the standard deviation. For the upper and lower limits, a bound of 3σ and -3σ was used, respectively. These bounds represented what the expected maximum and minimum values that the collected data should have fallen within.

For the statistical analysis, all of the tested devices fell within the $\pm 3\sigma$ deviation. This implied that all values for the boards were within the expected, statistical range for the measurements. In addition, the devices all demonstrated a consistent level of increase and leveling off for the same increments of time tested. This increase is substantial in the very early stages of the immersion, but after 5 d of immersion, this increase starts to decrease until a small, linear rate of increase is achieved. This pattern of rapid increase and then leveling off indicates that the devices quickly absorb water, but then absorb water less rapidly, as the circuit boards are approaching complete saturation. The

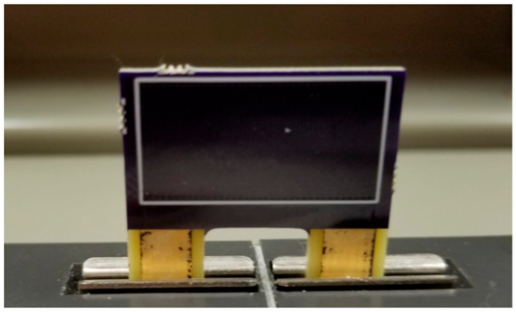

Fig. 6. Photograph of a sensor situated within the testing device.

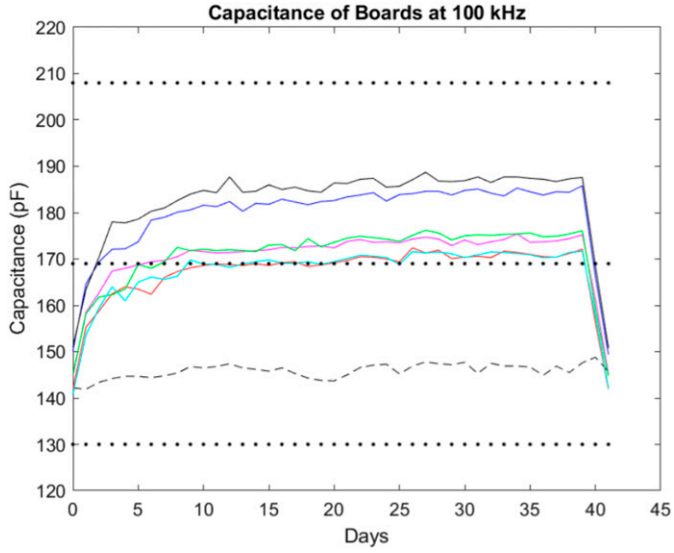

Fig. 7. Graph of the capacitance of the sensors at 100 kHz versus time.

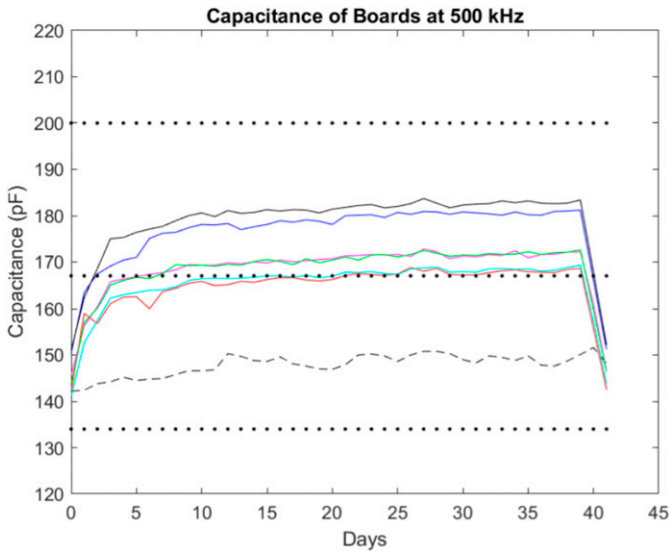

Fig. 8. Graph of the capacitance of the sensors at 500 kHz versus time.

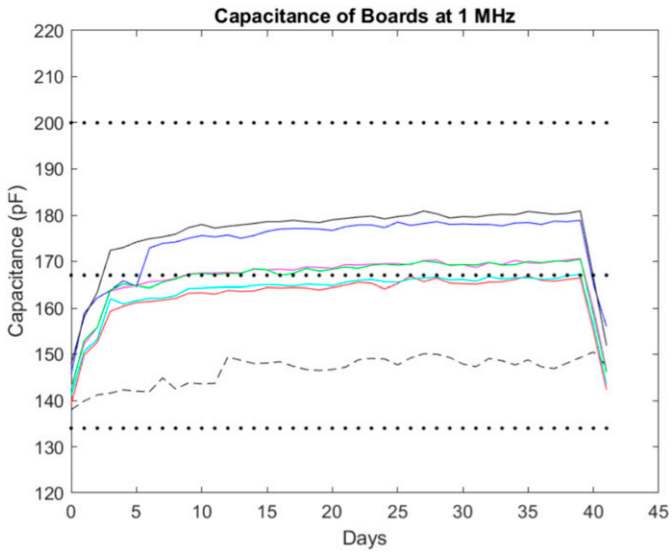

Fig. 9. Graph of the capacitance of the sensors at 1 MHz versus time.

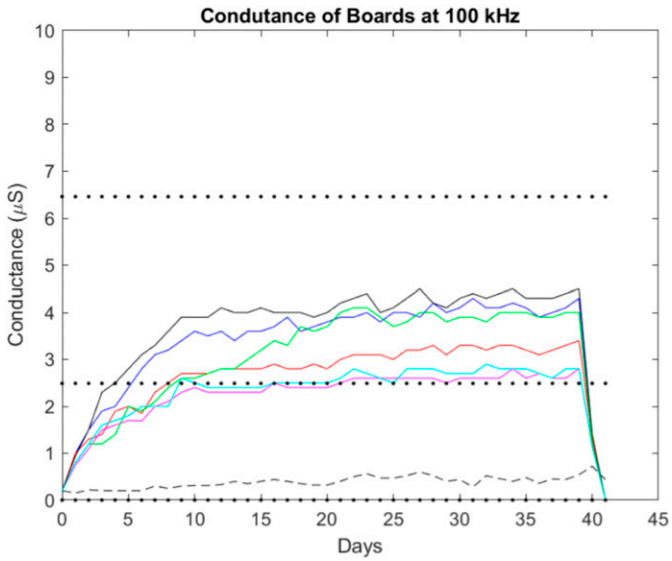

Fig. 10. Graph of the conductance of the sensors at 100 kHz versus time.

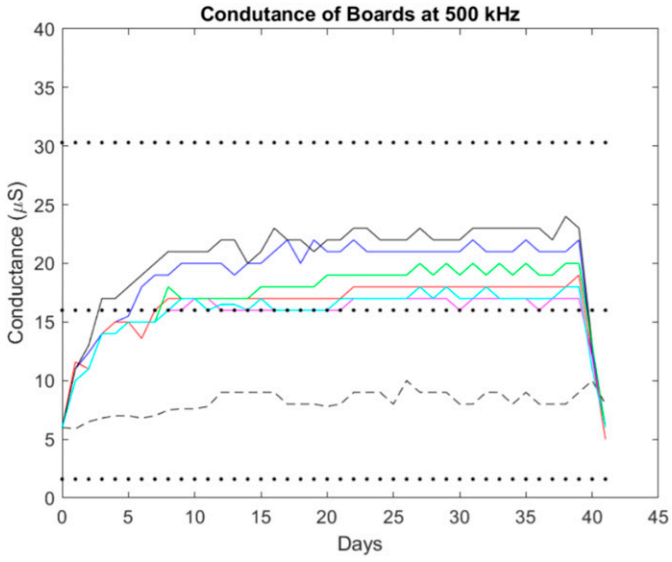

Fig. 11. Graph of the conductance of the sensors at 500 kHz versus time.

small increases measured during the leveling off are likely due to pockets in the circuit boards absorbing smaller amounts of water that did not initially absorb any water. Across all three frequencies, the values for the capacitance of each device were approximately the same. This is expected because the relative permittivity of water does not change substantially over the frequency range tested. For the conductance, at 100 kHz, the values typically peaked below 10 μS/m, whereas for the 500 kHz and 1 MHz measurements, the values were up to 20 μS/m. The boards also demonstrated a return to the original measured values after the posttest dehydration. The results of this dehydration can be seen as a sharp spike toward the originally measured values for each device at the end of each graph.

All of the sensors had an initial capacitance of approximately 140 pF. At the end of 42 d, the seven sensors that were immersed had capacitances between 160 and 180 pF, an increase of between 14% and 29%. Because the FR-4 and the solder mask had a relative permittivity of approximately 4, (1) yielded a capacitance of 5.97 pF. With the measured dry capacitance in air of 140 pF, (2) was used to determine a value for γ of 23.4. The reference sensor also experienced a slight increase in capacitance during this time, which was likely due to absorbing moisture directly from the air. The exposed sensors all experienced a substantial increase in electrical conductance during the 42 d of immersion. Because local tap water was used for these tests and not deionized(DI) water, to simulate a more realistic operating environment, the dissolved ions in the local tap water resulted in the large increase in electrical conductance observed. Once the immersed sensors were dehydrated, their capacitance and conductance values returned to approximately

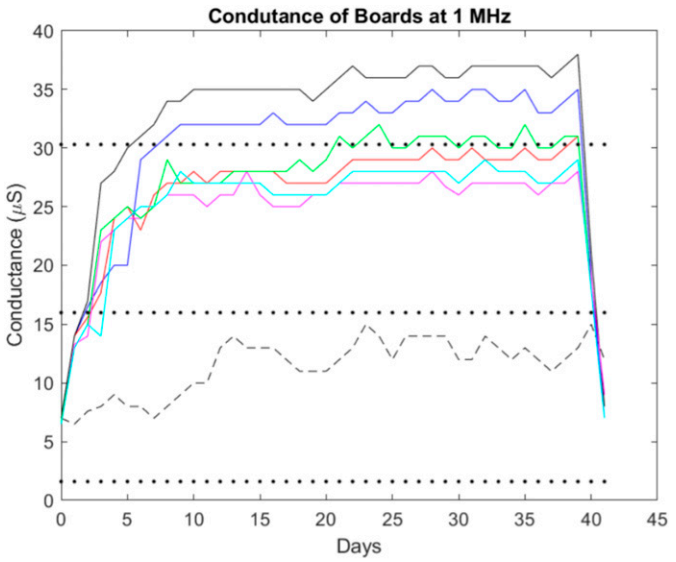

Fig. 12. Graph of the conductance of the sensors at 1 MHz versus time.

the same values as were measured initially. The rather large variation in capacitance measurements during the immersion testing is primarily attributed to variations in how the different circuit boards responded to the same immersion process, although all of the boards were from the same lot of commercially manufactured two-layer PCBs.

Conclusion

PCBs absorb moisture in moist operating environments, which can be detrimental to their performance. However, it is often difficult to determine that moisture absorption is occurring until a catastrophic failure occurs. To alleviate this issue, a moisture absorption sensor has been developed consisting exclusively of the standard materials and fabrication processes used to realize commercial PCBs. Seven sensors were evaluated through a prolonged immersion in water and demonstrated an increase in sensor capacitance of between 14% and 29%. These low-cost sensors could easily be added to most PCBs, only requiring a small amount of circuit board area and simple interface circuitry [1, 17].

References

[1] R.N. Dean, N.B. Loden, C.J. Hartley, and J.D. Craven, II, "An integrated sensor for detecting moisture ingress in printed circuit board assemblies," Proceedings of the IMAPS 49th International Symposium on Microelectronics, pp. 4, Pasadena, CA, 10-13 October 2016.

[2] D. Markus, M. Schmidt, K. Lunz, and U. Becker, "A new method to model transient multi-material moisture transfer in automotive electronics applications," Proceedings of the 17th International Conference on Thermal, Mechanical and Multi-Physics Simulation and Experiments in Microelectronics and Microsystems, pp. 8, Montpellier, France, 18-20 April 2016.

[3] H.A. Broadbent, S.Z. Ivanov, and D.P. Fries, "PCB-MEMS environmental sensors in the field," Proceedings of the 2007 IEEE International Symposium on Industrial Electronics, pp. 3282-3286, Vigo, Spain, 4-7 June 2007.

[4] J. Baskin, "Methods to mitigate contamination and moisture ingress in switchgear," Proceedings of the 2006 IEEE 11th International Conference on Transmission and Distribution Construction, Operation and Live-Line Maintenance, pp. 7, Albuquerque, NM, 15-19 October 2006.

[5] J. Kapur, J.L. Norwood, and C.D. Cwalina, "Determination of moisture ingress rate through photovoltaic encapsulants," Proceedings of the 2013 IEEE 39th Photovoltaic Specialists Conference, pp. 3020-3023, Tampa, FL, 16-21 June 2013.

[6] M.G. Pecht, H. Ardebili, A.A. Shukla, J.K. Hagge, and D. Jennings, "Moisture ingress into organic laminates," *IEEE Transactions on Components and Packaging Technologies*, Vol. 22, No. 1, pp. 104-110, 1999.

[7] S. Katsuki, R.P. Joshi, M. Laroussi, F. Leipold, and K.H. Schoenbach, "Electrical and optical characteristics of water under high electric stress," Conference Record of the Twenty-Fifth International Power Modulator Symposium, and High Voltage Workshop, pp. 467-470, Hollywood, CA, 30 June-3 July 2002.

[8] C.A. Balanis, "Electrical properties of matter," *Advanced Engineering Electromagnetics*, 2nd ed., John Wiley and Sons, Inc., Hoboken, NJ, 2012, pp. 39-98.

[9] A.P. Wallenberger and D.R. Lyzenga, "Measurement of the surface tension of water using microwave backscatter from gravity-capillary waves," *IEEE Transactions on Geoscience and Remote Sensing*, Vol. 28, No. 6, pp. 1012-1016, 1990.

[10] H.-C. Hsu, S.-J. Wu, F.-J. Hsu, M.-C. Weng, and S.-L. Fu, "Electrochemical migration failure on FR-4 PCB by hygro-thermo-vapor pressure coupled analysis," Proceedings of the 8th International Microsystems, Packaging, Assembly and Circuits Technology Conference, pp. 166-169, Taipei, China, 22-25 October 2013.

[11] H. Lobe, "Recent advances in biofouling protection for oceanographic instrumentation," Proceedings of MTS/IEEE OCEANS 2015, pp. 4, Washington, DC, 19-22 October 2015.

[12] R.N. Dean and F.T. Werner, "A PCB environmental sensor for use in monitoring drought conditions in estuaries," *Journal of Microelectronics and Electronic Packaging*, Vol. 13, pp. 182-187, 2016.

[13] R.N. Dean, A. Rane, M. Baginski, Z. Hartzog, and D.J. Elton, "Capacitive fringing field sensors in printed circuit board technology," Proceedings 2010 IEEE International Instrumentation and Measurement Technology Conference, pp. 970-974, Austin, TX, 3-6 May 2010.

[14] M.A.Md. Yunus, and S.C. Mukhopadhyay, "Novel planar electromagnetic sensors for detection of nitrates and contamination in natural water sources," *IEEE Sensors Journal*, Vol. 11, No. 6, pp. 1440-1447, 2011.

[15] A.S. Zoolfakar, N.H. Mahzan, A. Manut, and M.F. Idros,"Design, fabrication and characterization of a pH transducer using printed circuit board (PCB)," In Proceedings 2010 International Conference on Electron Devices, Systems and Apps., pp. 206-211, Kuala Lumpur, Malaysia, 11-14 April 2010.

[16] M.A. Md Yunus, M. Faramarzi, S. Ibrahim, W.A.H. Altowayti, and G.P. San, "Comparisons between radial basis function and multilayer perception neural networks methods for nitrate and phosphate detections in water supply," In Proceedings 2015 10th Asian Control Conference, pp. 1-6, Kota Kinabalu, Malaysia, 2015.

[17] Y. Meng and R.N. Dean, "A technique for improving the linear operating range for a relative phase delay capacitive sensor interface circuit," *IEEE Transactions on Instrumentation and Measurement*, Vol. 65, No. 3, pp. 624-630, 2016.

[18] A. Rivadeneyra, J. Fernandez-Salmeron, M. Agudo-Acemel, J.A. Lopez-Villanueva, L.F. Capitan-Vallvey, and A.J. Palma, "Printed electrode structures as capacitive humidity sensors: a comparison," *Sensors and Actuators A: Physical*, Vol. 244, pp. 56-65, 2016.

[19] R.N. Dean, A.R. Rane, M.E. Baginski, J. Richard, Z. Hartzog, and D.J. Elton, "A capacitive fringing field sensor design for moisture measurement based on printed circuit board technology," *IEEE Transactions on Instrumentation and Measurement*, Vol. 61, No. 4, pp. 1105-1112, 2011.

[20] M. Uematsu and E.U. Frank, "Static dielectric constant of water and steam," *Journal of Physical and Chemical Reference Data*, Vol. 9, No. 4, pp. 1291-1306, 1980.

[21] R.N. Dean and A.K. Rane, "A digital frequency-locked loop system for capacitance measurement," *IEEE Transactions on Instrumentation and Measurement*, Vol. 62, No. 4, pp. 777-784, 2013.